Thorsten Pofahl, Alex Seiter, Martin Trautz, Lisa-Marie Reitmaier, David Baill, Gerhard Hirt

# Form Finding of a Sheet Metal Shell by Generative Design and Pareto Optimization

**Abstract:** The study focuses on the design and optimization of a shell structure made from a 1 mm thick aluminum sheet. The objective of the research is to create an optimized structure that meets the requirements of structural performance, material usage, and production efficiency. We employed a generative definition for the structure and implemented a multi-criteria optimization approach to balance conflicting objectives. The structural morphology of the shell is considered on both macro and micro scales. At the macro scale, various shell shapes, ranging from simple spherical domes to undulated shells with different cross-sections, are explored. The shape of the shell is optimized to achieve both structural performance and production efficiency. Undulating the shell edge is found to positively impact the structural behaviour, although it increases the complexity of the components. On the microscale, structural embossments in the form of beads are introduced to enhance the moment of inertia, buckling resistance and natural frequencies. A parametrically defined bead arrangement is employed resulting in various patterns. The optimization process follows a multi-objective approach, aiming to simultaneously optimize structural performance, tool material usage, and production time. The objectives are derived from the geometry itself or calculated through a linear buckling analysis. The optimization is not weighted initially, allowing all objectives to carry equal priority. The solutions are then represented in non-normalized result domains and Pareto surfaces to evaluate their performance and compatibility. Through the analysis of 22 generations and 4400 parameter sets, the research provides insights into load-bearing capacity, serviceability, manufacturing effort, and manufacturing costs. The results highlight the trade-offs between different objectives and the interplay between shell geometry, stability, and production parameters.

## 1 From sheet metal to shells

The basic design for the demonstrator is a circular shell on 5-point supports with a diameter of 4.2 m, made from a 1 mm thick aluminum sheet. See Fig. 1 for design and Fig. 2 for production process. We adapted stretch forming and incremental sheet forming processes to produce the complex sheet metal components [1, 2]. Both the overall shape and structural detailing adapt to these primary constraints and are optimized in terms of structural performance, material usage and production efforts. We implemented a generative definition for the structure with a broad spectrum of possible forms and as few input parameters as possible. The analysis procedures are


https://doi.org/10.1515/9783111162683-028

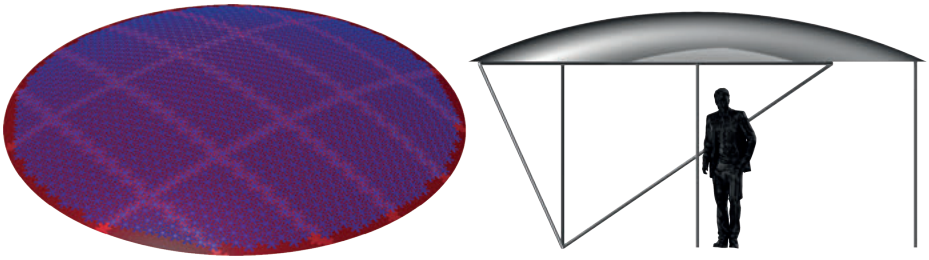

**Fig. 1:** Demonstrator design in view, perspective, and detail.

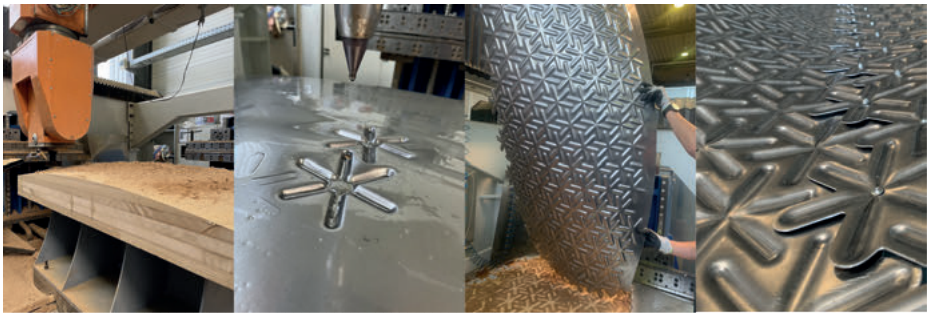

**Fig. 2:** MDF tool block adapts geometry, IBU forming tool traces beads, finished component, Panel joint with pattern overlay.

fully integrated and allow for the usage of an evolutionary algorithm to find reasonable conditions for our design, each balancing opposing goals differently. Based on this set of solutions, we derived general observations on the overall behavior and principles of our system.

## 2 Structural morphology

Structural morphology is the overall consideration of form, structure and forces. It is a non-hierarchical design principle on different scales [3]. In our case, we are considering the macro-structure of the shell at the global scale and the individual structural embossments at the local scale. The overall optimization on all scales results in the optimal "layout", which includes information about the topology, shape, size of the structural components, and materiality. Optimization processes that address several objective functions simultaneously are used to search for the optimal "layout", following the abstraction of natural processes [4]. The principles of structural morphology guide the adjustment of the basic topology of the shell shape and bead pattern, using a global optimization process that considers both structural behaviour and production

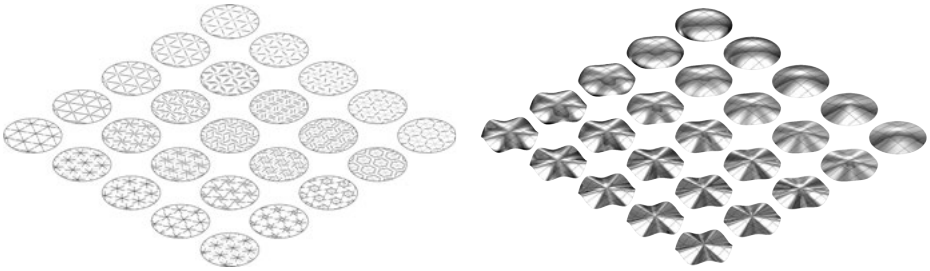

**Fig. 3:** Microstructures (left), macrostructure (right).

effort. Rather than being combined in an objective function with a priori weights, these partially conflicting objectives are examined in a multi-criteria process, resulting in a solution set of structural variants that fulfill different objective criteria with varying weightings. This approach allows for the individual components of the problem definition to be derived from the composition of the solution set and for the optimization goals to be weighted based on a multitude of conceivable solutions.

## 2.1 Macroscale – shell structure

The spectrum of possible shell shapes ranges from a simple spherical dome to a multi-curved undulated shell shape with linear or parabolic cross-section. A spherical dome allows all components to undergo stretch-forming on identical or nearly similar molds. The only differences between components are in their cut and pattern formation. Adapting the mold to the next shape to be produced by milling results in a minimum of mold material and production time. Although this shell geometry is not necessarily the optimum shape from a structural point of view, creating the shape based on a parabola or catenary can lead to improved structural behaviour. Undulating the shell edge results in a rotationally symmetrical alternation of synclastic and anticlastic curvature changes, which can also positively impact the structural behaviour (Fig. 3, right). However, both measures increase the degree of component complexity. The complexity is measured by the volume of the required tool block into which the part geometries are oriented and sorted (Fig. 4, left). To represent as wide a spectrum of shapes as possible with a minimum number of parameters, a parametric definition of the shell was developed in this investigation. The parametric definition of the form is based on radial longitudes, which are defined as a basic spline curve and adjusted through variation of three control points. In the radial coordinate system of the sphere, the $x$-component of the center point influences the shell cross-section and is defined as a variable (Fig. 4, right, in green). The undulation is achieved by adjusting the $z$-component of the curve end point at every second curve (Fig. 4, right, in red).

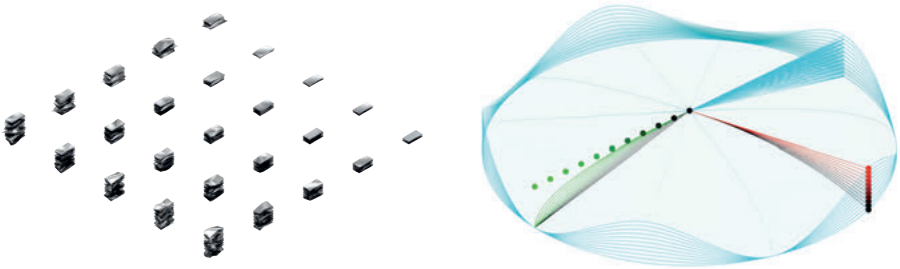

**Fig. 4:** Parameters of the local and microscale.

## 2.2 Microscale – structural embossments

Beads are predominantly utilized to fulfill utility functions such as enhancing the moment of inertia, buckling resistance and natural frequencies ($\omega k$), as well as modifying reaction forces and moments [5,6]. In the context of structural morphology, beads serve as the additional structural elements at the local scale. The arrangement of individual beads creates basic shapes, which are then patterned in relation to each other. The degree of additional global bending stiffness induced by the beads relies on the base shape, pattern, and pattern density. A parametrically defined pattern is employed in this investigation. The definition allows a seamlessly transformation of the patterns, resulting in a kaleidoscopic effect in the superposit. The pattern definition is based on a triangle mesh, where truncated edges are rotated around a movable point. One of the parameters of this definition is the rotation angle, which varies between 0 and $0.5\,\pi$. Another parameter determines the point on the length domain, about which the edge is rotated. Based on these two parameters, a spectrum of patterns representing triangular and hexagonal meshes, with linear, star-shaped and elemental properties and different degrees of entanglement can be generated (Fig. 3, left). Entanglement of the patterns is equivalent to the elimination of axes without significant moments of inertia. It is important that the patterns are interlocked in at least two perpendicular directions, preferably in three axes intersecting at 60°. The greater the entanglement, the more continuous the bending stiffness and the more homogeneous the component. A third parameter scales the mesh within a domain of 100–200 %. The production time of these patterns is directly proportional to the total length and complexity of the forming paths of the milling and forming tool.

# 3 Multi-objective optimization

A multi-objective optimization is an optimization problem with multiple objectives [7]. It can be written as:

$$\min_{x \in X} = (f_1(x), f_2(x), \ldots, f_k(x))$$

With $k \geq 2$, $k \in N$ as the number of objective functionals, and the set $X$ as the admissible set of the explorable set, which is usually $X \in R^n$ but depends on the $n$-dimensional input domain. The admissible set is usually defined over bounded functions. The vector objective function:

$$f : X \to R^k,\ x \mapsto (f_1(x), f_2(x), \ldots, f_k(x))$$

If an objective function is to be maximized, the negative or the inverse is minimized. We set: $Y \in R^k$ as a mapping of $X$, $x^* \in X$ as an admissible solution, and $z^* = f(x^*) \in R^k$ as a result. In Multi-Objective Optimization, there is usually no admissible solution that minimizes all objective functions simultaneously. The solution is done by considering a Pareto-optimal solution. This means none of the objectives can be improved without worsening at least one objective. An admissible solution $x_1 \in X$ is Pareto-dominant over a solution, $x_2 \in X$ if:

$$\forall i \in \{1, \ldots, k\},\ f_i(x_1) \leq f_i(x_2) \text{ and } \exists\, i \in \{1, \ldots, k\},\ f_i(x_1) < f_i(x_2)$$

The solution $x^* \in X$ (and the corresponding result $z^* = f(x^*)$) is called Pareto-optimal if there is no more dominant solution. The set of Pareto-optimal solutions written as $X^*$ is the Pareto front (3D Pareto surface).

## 3.1 Implemented objective functions

The optimization problem sets high structural performance, minimum tool material usage, and short production time as objectives. The values of these objectives are derived from the geometry itself or calculated through a linear buckling analysis.

$z_1$ = value of deformation = stiffness of the system

$z_2$ = value of instability = −1/load factor

$z_3$ = value of the IBU pathlength = forming time

$z_4$ = value of tool material = milling + material effort

For each generation of the optimization, the following result domains are created.

$$\min z_i = \min\{z_i\} \text{ und } \max z_i = \max\{z_i\},\ D_i(z_i) = [\min z_i; \max z_i]$$

Normalized to domain [0; 1] for result representation and interpretation:

$$z_i^n = \frac{z_i - \min z_i}{\max z_i - \min z_i},\ \max z_i = \max\{z_i\},\ D_i^n(z_i) = [\min z_i^n; \max z_i^n] = [0; 1]$$

The optimization is not weighted, indicating that all objectives carry the same priority. Subsequently, the results can be manually weighted later. Moreover, it is feasible to eliminate solutions in case the result values surpass or fail to meet specific threshold values.

## 3.2 Geometric evaluation (Grasshopper)

We used the Rhinoceros Grasshopper environment (GH) for the overall process chain, including geometrical evaluation. To evaluate the material requirements for forming tools, we first fit the panels into the stretch forming machine's installation space in a production-friendly manner and sort them into a compact volume, which requires optimization based on a traveling salesman problem (TSP). Then, we compute the tooling and material efforts for successively milling individual forming tools from this volume: $h(V_{\min}) = z_4$. To determine the forming time, we sum up the individual lines of the patterns (= milling paths) to obtain a total length. The forming time equivalent to the path length: $\sum_{i=1}^{n} L_i = z_3$.

## 3.3 FEM (Karamba)

Thin shell structures, akin to thin compression members, are typically evaluated based on their stability, rather than the stress in their cross sections. In the state of membrane stress, significant strain energy can be stored without much deflection. However, if this energy is converted into bending energy, it can lead to instabilities and result in a loss of load-bearing capacity [8, 9]. Consequently, the maximum deflection of the structure with Th. II. O. under a constant area load, as well as the load factor of the structure, which is determined by a linear buckling analysis (LBA), are used to assess the structural performance of the shell structure. Nonlinear analyses (GNA, GNIA, or GNMIA) that provide more accurate results are not considered since the ranking of the results within the solution domain is decisive, rather than the absolute values themselves. Additional information on model building can be found in references [10, 11]. The beads are represented by bar elements joined with hinges. The calculations are carried out within GH, using the finite element (FE) method with the Karamba plug-in. The automatically obtained maximum deflection is: $\max u_z = z_1$. Linear buckling analysis is the solution to an eigenvalue problem based on: $(K + \lambda_i K_g)\Psi_i = 0$, where $K$ is the (linear elastic) stiffness matrix, $K_g$ is the geometric stiffness matrix calculated for a reference load, $\lambda_i$ is an eigenvalue (load factor), and $\Psi_i$ is a corresponding eigenvector

(buckling shape). The LBA assumes negligible deflections before the bifurcation of the load path (not the case for nonlinear consideration). The lowest eigenvalue is referred to as the critical load factor $\lambda_{kr}$ [8]. For the load factor (negative because the maximum of the objective function is searched for), the following applies consequently: $\lambda_{kr} = -z_2$.

### 3.4 Optimization (Octopus)

The optimization problem is solved with the Octopus plug-in within GH. The plug-in is based on the evolutionary algorithm HypE. This algorithm contains a fitness assignment scheme based on the Lebesgue measure and can both compute this measure exactly or estimate it using Monte Carlo sampling. The estimation allows a compromise between fitness accuracy and computation time, which makes hypervolume-based search feasible even for problems with many objective functions [12].

## 4 Results

A total of 4400 parameter sets were calculated over 22 generations, with each generation consisting of 200 sets. Subsequently, various result representations are analyzed to draw general conclusions and identify phenomena.

### 4.1 Non-normalized result domains

The non-normalized result domains indicate the potential range of solutions for each objective function. They cannot be directly combined or weighted. Nevertheless, they provide insight into loadbearing capacity, serviceability, manufacturing effort, and manufacturing costs. Moreover, the results can be roughly weighted based on these estimates. The non-normalized result domains of the individual objective functions are as follows:

$$z_1 = \text{value deformation} = [0.01 \ldots 3.20]\,\text{cm}$$
$$z_2 = \text{value stability} = [0 \ldots 90]$$
$$z_3 = \text{value IBU pathlength} = [243 \ldots 498]\,\text{m}$$
$$z_4 = \text{value tool + material} = [0.11 \ldots 2.08]\,\text{m}$$

### 4.2 Pareto surface(s)

In the present study, there are four objective functions. To represent a Pareto surface in Cartesian space, the results of three of the objective functions can be plotted on

the three axes ($x$, $y$, $z$). Figure 6 (left) shows the solutions depending on the objective functions, tool material, stability, and IBU from the first (red dots) to the last generation (white dots). The result ranges are normalized. The Pareto surface is also shown for the last generation. Based on the plot, the following can be determined:

- The higher the generation, the more two-dimensional the solution space becomes due to the IBU path ($z_3 \rightarrow 0$).
  $\Rightarrow$ Many Pareto-optimal solutions achievable with less IBU.
- Still, the most stable systems ($z_2 \rightarrow 0$) require the longest IBU paths ($z_3 = 1$).
  $\Rightarrow$ A high density of indentations leads to stable systems.
- The most stable systems ($z_2 \rightarrow 0$) can have low demand for tooling material ($z_4 = 0$).
  $\Rightarrow$ Simple shell geometries can be stable.
- In the Pareto-optimal solutions, there are many results with a low IBU path length ($z_3 \rightarrow 0$). Many of these solutions have a low tool material requirement ($z_4 \rightarrow 0$) too. These solutions are not very stable ($z_2 \rightarrow 1$).
  $\Rightarrow$ Simple shell geometries with low density of indentations lead to unstable systems.

One can identify the extent to which the objectives can be achieved and the strength of their compatibility. Additionally, it is possible to determine whether the optimization converges. Choosing the best candidate is proven to be difficult, and no conclusions can be drawn regarding the system's geometry dependencies.

## 4.3 Multi-axis representation

In this representation, we define each objective function one-dimensionally using its respective $y$-axis, onto which the solution results are plotted. The results of a given solution are then connected by a line, yielding a polyline for each solution (Figure 5). This creates a representation that is one-and-a-half-dimensional in nature, effectively summarizing the individual objective functions much like a stock market curve. It's worth noting that the optimal solution would be $f(x) = 0$.

A. This graph is equivalent to Fig. 4 but plotted in one-and-a-half-dimensional space. The scales have been normalized, with 0 representing optimal performance and 1 indicating suboptimal performance. Result variance is observed to decrease at higher generations, except for the objective stability (which remains unchanged). This trend is particularly pronounced in the case of Pareto-optimal solutions, which are dominated by minimal deflection and IBU values (with a few outliers for IBU). Additionally, the variance of used tool material is approximately half that of stability.
   $\Rightarrow$ IBU and deflection are dominant.

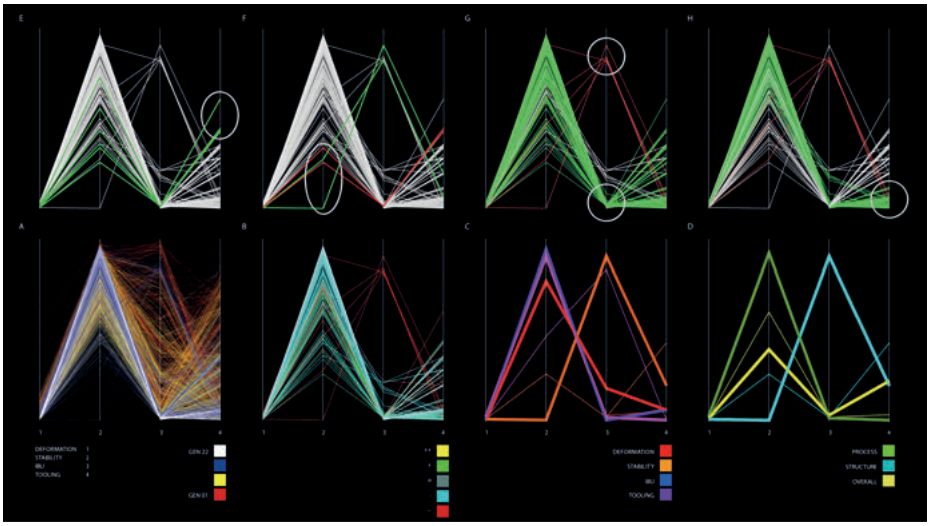

**Fig. 5:** Multi-Axis representation.

B. In this graph, the Pareto-optimal solutions of the last generations are plotted. However, an evaluation of the solutions is done here: All results $f(x_i) \in [0; 1]$ of a solution are summed up: $\sum_{i=1}^{4} f(x_i)$. The solution with the minimum sum value is the best (++, yellow), with the maximum sum value the worst (– –, red). The solutions with high IBU are the worst within the Pareto-optimal solutions. All the best results have minimum IBU.
⇒ IBU is dominant.

C. The graph shows the first- and second-place optima of the last generation with the respective minimum results of the individual objectives. We observe that the Pareto-optimal solution with the best stability also possesses the poorest IBU and tool material values of all such solutions. Furthermore, the remaining Pareto-optimal solutions, each of which has a single minimum value, exhibit very poor stability values. Intriguingly, the solution characterized by maximum stability proves to be among the worst performers. However, the second most stable solution performs quite well across all metrics. We conclude that the best solutions are those that minimize deflection and IBU, exhibit good-to-moderate stability, and employ tooling material in a sparing-to-very-sparing fashion.
⇒ Stability and IBU, as well as stability and tool material, behave contrary to each other. ⇒ IBU and tool material behave equivalently.

D. This diagram combines IBU and material cost into a single “process” objective, while deflection and instability are grouped together as the “structure” function. A third curve provides a comparison to the overall view displayed in Graph B by showing the optimum solution.

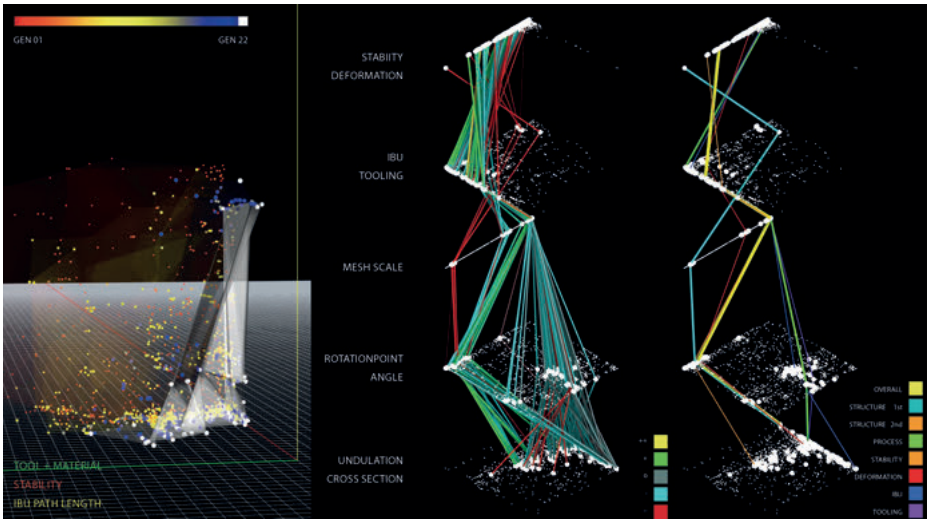


**Fig. 6:** 3D solution space pareto surfaces of all generations (left), Parameter-Referenced Multi-Level representation (middle and right).

- Structure solution corresponds to the best performing stability solution, which also exhibits very good deflection properties.
- Process function behaves according to the partial parameter curves.
- The generalized function achieves very good IBU and deflection properties, as well as average stability and tool characteristics.

Graphs E-H depict the curves from the most recent generation, with each graph highlighting a different subset of the Pareto set. These subsets were selected based on specific criteria, which are marked by circles and ovals.

E. Stability exhibits a wide spectrum; stability is achieved by much IBU (green) or high use of tooling material (red).
F. Much IBU is used when usage of tooling material is low (red), and the algorithm prefers less IBU, despite fluctuating results of the remaining objective functions (green).
G. High usage of tool material leads to stable systems, even with low IBU.
H. Low usage of tool material leads to low stability (green), except combined with much IBU (red).

## 4.4 Parameter-referenced multi-level representation

This form of representation aims to gain insights into the interdependencies of geometrical parameters and objectives by combining input parameters and target values (Fig. 6). It is divided into five diagram levels that summarize related values and display them as white dots. The domains of the representation levels are normalized over the results of the total solution space, and all values set and achieved in the optimization process are displayed as smaller dots. Each solution of the last optimization generation is represented as a polyline that links the corresponding solution and objectives. The lower three levels of the diagram depict the parameters for the shell geometry, pattern, and scaling and can be directly linked to the graphical representation in Fig. 3 and Fig. 4 while the upper two levels display the objectives. The upper diagram combines the structural objectives of deflection and stability, while the lower diagram shows the process objectives of tool material consumption and IBU process time. The zero value, or optimal solution, is located at the leftmost point of each diagram. Figure 6 displays the input and result values from Figure 5B, with the 131 solutions from the last optimization generation weighted by the sum of their target values and shown in color. The best solution is represented by yellow, while green represents good results, turquoise represents average results, and red represents poor results. This representation allows for conclusions to be drawn about the structural forms of the final solution space and their overall structural and process performance. The input parameters exhibit a strong containment pattern.

- Many shell shapes have an arbitrary cross-section and lack undulation. However, shells based on circular cross-sections with medium undulation perform better.
- Discontinuous triangular meshes are the predominant pattern and tend to score better. Strongly entangled three-rayed stars in various forms also appear frequently.
- Six-sided polyhedra play a less significant role.
- Pattern scaling shows a strong tendency towards low values (big stars), with only a few outlier solutions having high scaling (small stars).
- The result space for production targets is strongly limited, particularly with regards to the use of IBU, where most solutions use the minimum amount. However, some outliers rely heavily on IBU, including the best-performing solution structurally.
- In the solution space for structural parameters, the one-dimensional confinement is easily explained by the form-finding of shells. Through optimization, the total deflection was significantly reduced, but the spectrum of achieved stabilities is almost completely covered by the initial range of solutions.

In Fig. 6 (right), a subset of the variants that correspond to Figures 9C and 9D is displayed. The input parameters exhibit high variance in the partial selection, making it advisable to interpret the structural shapes depicted in Fig. 7, which shows the shell geometries bead pattern and buckling shapes.

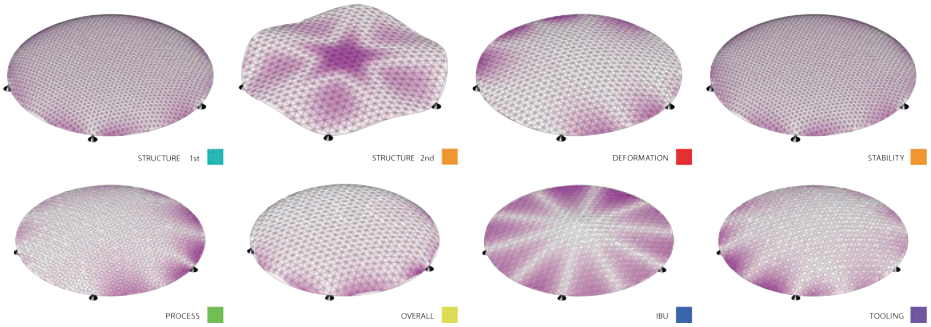


**Fig. 7:** Geometries of best solutions (buckling spapes).

- All variants except for a few outliers have a pattern of six-sided stars with non-intersecting rays aligned with the base network.
- The elliptical profile (shown in structure 1st in Fig. 7) provides a classic stiffening effect at the free edge, resulting in high stability. Changing from an elliptical profile to a linear one leads to a significant loss of stability but only a slight improvement in deflection performance.
- Dense patterns (shown in stability 1st in Fig. 7) contribute to stability.
- Shell geometries without undulation are dominant, except for the second-best result in static performance. The best solution for deflection has a parabolic to linear profile, which is equivalent to a suspension shape for point-supported shells with attachable bending stiffness. In this case, aclassic stiffening effect at the free edge is not necessary.
- Figure 7 indicates that the deflections of the best solutions are small relative to the total domain, suggesting that in the overall analysis, deflection is not the most crucial factor. This aligns with the assumption that for thin shells, stability issues related to static performance dominate.

# 5 Summary

The study presents a form-finding process based on the principles of structural morphology that optimizes the macro- and microstructure of the shell without hierarchy. Interpreting the results is fairly complex, due to the number of input parameters and objectives. Despite this, we observe clear tendencies in both shell shape and pattern generation, as well as deviating structural variants that highlighted trade-offs and reciprocal relationships: The solution space for this study includes both undulated and non-undulated options. Upon evaluation, many solutions with slight to medium undu-

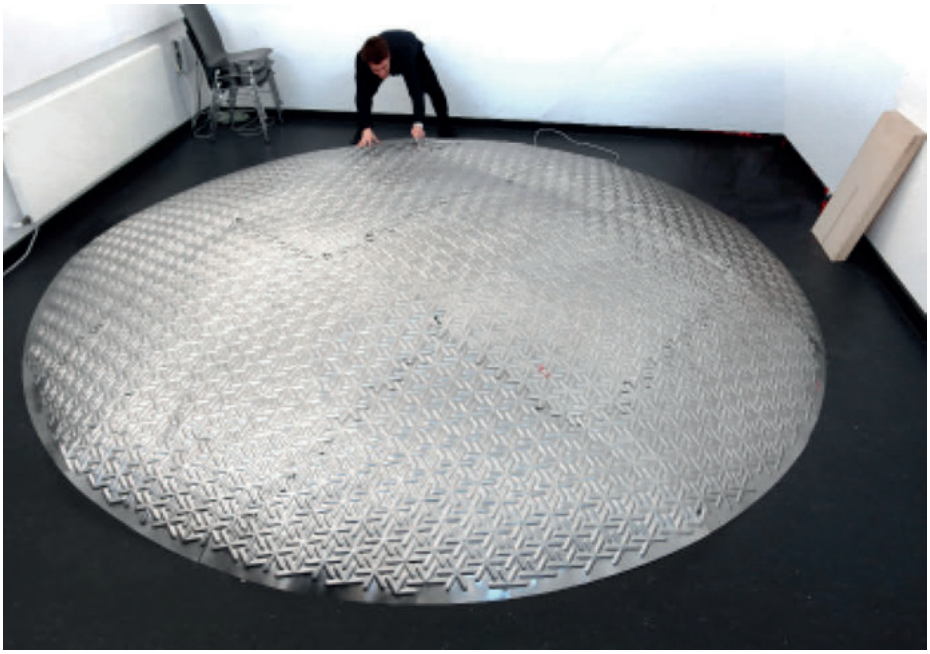

**Fig. 8:** Assembled Demonstrator.

lation and a specific cross-section (between circular and parabolic) fall within the good range. Interestingly, the best solutions are not undulated and cover the entire range of cross-sections, except for the best solution for structural performance. Regarding patterns, clustering can be observed in the solution space. Discontinuous patterns that map the axes of the grid tend to perform better than geometrically interlacing ones, representing the best results. However, there are still many solutions with interlacing triangular stars and hexagonal patterns with closed contours that perform moderately well. Coarse scaling appears to produce clear improvements. Good solutions are achieved with low use of IBU. In terms of structural performance, all results exhibit low deflection. However, the range of solutions for stability could not be narrowed down. Interestingly, the best performers in process and structure tend to perform poorly in the other area, leaving the overall solution space quite large. Nonetheless, many variants perform well in both process and structure metrics, showing that solutions that meet both criteria can be found through trade-offs. Surprising results from this study include how little the solution spaces could be narrowed down. Additionally, entangled patterns do not necessarily lead to the best performers in stability. Fig. 8 shows the assembled demonstrator.

## References

[1] Trautz, M., T. Pofahl, A. Seiter, G. Hirt, L.-M. Reitmaier, and D. Bailly. (2022). Karosseriebautechnik für die Architektur. Detail, H. 7./8. 2022, 22–24.
[2] Trautz, M., T. Pofahl, A. Seiter, G. Hirt, L.-M. Reitmaier, and D. Bailly. (2022). Leichtbaukonstruktionen aus Feinblech. Stahlbau 91, H. 6, 375–84.
[3] Motro, R. M. (2009). *Structural Morphology and Configuration Processing of Space Structures,* Multi-Science Publishing Co Ltd.
[4] Stach, E. (2010). Structural morphology and self-organization, Design and Nature, Pisa Italien, 29–40.
[5] Widmann, M. (1984). *Herstellung und Versteifungswirkung von geschlossenen Halbrundsicken,* Springer Berlin.
[6] Emmrich, D. (2005). Entwicklung einer FEM basierten Methode zur Gestaltung von Sicken für biegebeanspruchte Leitstützstrukturen im Konstruktionsprozess, F.-bericht Nr. 13 IPEK.
[7] Miettinen K. (1999). *Nonlinear Multiobjective Optimization.* Springer
[8] Aksel'rad, Ė. L. (1983). *Schalentheorie.* Stuttgart: Teubner.
[9] Kollár, L., and E. Dulácska. (1975). *Schalenbeulung.* Düsseldorf, Werner Verlag,
[10] Seiter, A., T. Pofahl, M. Trautz, L.-M. Reitmaier, D. Bailly, and G. Hirt. (2020). Metal Shells, 14. *Baustatik – Baupraxis.* 23.–24. März 2020, Universität Stuttgart, 439–46.
[11] Seiter, A., T. Pofahl, M. Trautz, L.-M. Reitmaier, D. Bailly, and G. Hirt. (2019). Design and Analysis of Freeform Shell Structures Composed of Doubly Curved Sheet Metal Panels. *Form and Force: IASS Symposium 2019,* 60–67.
[12] J. Bader and E. Zitzler. HypE: (2011) An Algorithm for Fast Hypervolume-Based Many-Objective Optimization. *Evolutionary Computation,* 19(1):45–76.